Physicochem. Probl. Miner. Process., 61(5), 2025, 210737

http://www.journalssystem.com/ppmp

Physicochemical Problems of Mineral Processing

ISSN 1643-1049

Enhancing the depression of pyrite flotation with potassium permanganate and 120 kHz ultrasonication

Lingpan Du [1], Jiangli Li [1], Menglai Wang [1], Fengting Zhao [1], Chang Lu [1], Qinbo Cao [2], Peilun Shen[2,3]

[1] Yunnan phosphate chemical group Co., Ltd

[2] Faculty of Land Resources Engineering, Kunming University of Science and Technology, Kunming 650093, Yunnan, China

[3] Innovation Center of Phosphorus Resource, Yunnan Province, China

Corresponding author: qinbocao@kust.edu.cn (Qinbo Cao)

Abstract: The separation of pyrite (FeS_2) from chalcopyrite ($CuFeS_2$) by froth flotation remains challenging in high-sulfur ore systems. Although potassium permanganate ($KMnO_4$) strongly depresses pyrite flotation, further improvement of its depression capacity is necessary. This study proposes a novel technique combining 120 kHz ultrasonication and $KMnO_4$ to inhibit FeS_2 flotation. Flotation experiments evaluated the ultrasonic effects on FeS_2 depression, whereas surface characterization clarified the underlying mechanisms for the FeS_2-$CuFeS_2$ system through contact angle measurement, zeta potential analysis, X-ray photoelectron spectroscopy, and scanning electron microscopy. Flotation tests demonstrated that 1 min of combined conditioning effectively reduced pyrite recovery to 27.81%, significantly lower than that with $KMnO_4$ alone (4 min). $CuFeS_2$ flotation by xanthate was unaffected after ultrasonication. Zeta potential analysis revealed that ultrasonication markedly increased FeS_2 surface oxidation, thus reducing xanthate adsorption. Furthermore, FeO, FeOOH, and SO_4^{2-} formed on the FeS_2 surface after combined treatment, explaining the effective depression. These findings broaden ultrasound applications in mineral separation.

Keywords: ultrasound, pyrite, separation, froth flotation, synergistic effect

1. Introduction

Pyrite (FeS_2) is a common sulfide found in nonferrous metal sulfide ores, frequently coexisting with other sulfide minerals within the same mine (Zhang et al., 2023). Especially for copper sulfide ores, where chalcopyrite ($CuFeS_2$) typically represents the primary Cu-bearing mineral, FeS_2 is more abundant. Due to its low economic value, FeS_2 is generally regarded as a gangue mineral and is relegated to tailings in processing plants (Owusu et al., 2014). Therefore, the complete removal of FeS_2 from $CuFeS_2$ ore is essential to satisfy the requirements of copper smelting (Khoso et al., 2019).

Extensive efforts have been undertaken to develop novel FeS_2 depressants (Wu et al., 2022). Nevertheless, lime remains the predominant depressant in industrial practice, primarily due to its low cost in China (Feng et al., 2019; Hassanzadeh and Hasanzadeh, 2017; Liu et al., 2020). Lime can adjust the slurry pH to between 9 and 10, thereby inducing certain redox reactions on the FeS_2 surface (Bai et al., 2021; Yan et al., 2018; Zanin et al., 2019). Besides, calcium hydroxide species can adsorb onto the FeS_2 surface (Chen et al., 2011), thereby inhibiting FeS_2 flotation. Lime is typically introduced into grinding mills to enhance its depression capability by interacting with fresh FeS_2 surfaces, given its low solubility. However, in some instances, complete depression of FeS_2 cannot be achieved when abundant finely disseminated FeS_2 is present in the ores.

To address the limitations associated with lime, various inorganic and organic depressants have been employed to significantly depress FeS_2. Most inorganic reagents function as oxidizers, reacting with pyrite to form oxidative hydrophilic species. For example, H_2O_2 interacts with FeS_2, producing FeO/FeOOH products that inhibit collector adsorption at Fe sites on the FeS_2 surface (Khoso et al., 2019). Organic depressants for sulfide minerals have attracted substantial attention in recent years. These depressants typically consist of macromolecular polymers containing C−O and OH functional

DOI: 10.37190/ppmp/210737

groups (e.g., biopolymers (Mu et al., 2018) and starch (Han et al., 2019)). These polymers exhibit high hydrophilic-lipophilic balance (HLB) values. The presence of such polymers on the FeS_2 surface directly enhances its hydrophilicity. However, the application of organic reagents in industrial settings remains limited due to their sensitivity to slimes and poor selectivity for sulfides (Cao et al., 2023b). Therefore, the depression of FeS_2 necessitates the development of innovative reagents and techniques.

Potassium permanganate ($KMnO_4$) has been established as an effective depressant for pyrite. $KMnO_4$ is a potent oxidizing agent (E^0 = 0.59 V) and poses significant environmental concerns. However, its environmental effects can be mitigated in industrial applications, as water containing $KMnO_4$ may be recycled in a closed flowsheet through pulp sedimentation and dewatering processes. Nonetheless, improvements in the depression efficiency of $KMnO_4$ are necessary, such as reducing both its reaction time and dosage, to minimize environmental hazards. Recent studies have demonstrated that ultrasonic irradiation at 120 kHz significantly enhances the interaction between sulfuric acid (H_2SO_4) and galena, reducing the H_2SO_4 reaction time from 14 min to 6 min (Cao et al., 2024a). It is generally accepted that ultrasound induces cavitation within a solution (Mitra et al., 2021), creating localized hotspots (approximately 5000 K) that accelerate surface oxidation kinetics (Ashokkumar, 2011; Ashokkumar et al., 2000; Ashokkumar and Grieser, 2005; Nie et al., 2021). Ultrasound treatment has been successfully used in some mineral flotation systems, such as goethitic (Marques et al., 2025), sulfide ores (Celik, 1989; Gungoren et al., 2020), quartz (Gungoren et al., 2019), potash (Filippov et al., 2021), and graphite (Barma et al., 2019). Previous studies utilizing lower frequencies (<120 kHz) have indicated that ultrasonic treatment can effectively remove oxidative species from mineral surfaces through the effect of strong microjets traveling at 100 m/s (Altun et al., 2009; Celik, 1989). Differently, higher frequency ultrasound appears to facilitate mineral oxidation. However, it remains uncertain whether 120 kHz ultrasonication can enhance the oxidation capacity of $KMnO_4$ for FeS_2.

In this study, ultrasound at 120 kHz was employed during the $KMnO_4$−FeS_2/$CuFeS_2$ reaction to examine its effects on the separation of the two minerals. Initially, the impacts of combined ultrasound and $KMnO_4$ treatment on the flotation behavior of FeS_2 were evaluated through flotation tests. Furthermore, contact angle and zeta potential measurements were conducted to assess the hydrophobicity and zeta potentials of the mineral surfaces conditioned with ultrasound and $KMnO_4$. In addition, the oxidative components present on the FeS_2 surface were analyzed using X-ray photoelectron spectroscopy (XPS) and scanning electron microscopy (SEM).

2. Materials and methods

2.1. Minerals and reagents

FeS_2 and $CuFeS_2$ crystals of high purity were selected from a sulfide mine located in Yunnan province, China. The X-ray powder diffraction (XRD) data for these samples are illustrated in Fig. 1. The XRD spectra exhibited only the characteristic peaks corresponding to FeS_2 and $CuFeS_2$. Moreover, the X-ray fluorescence (XRF) results (Table 1) indicated that the FeS_2 sample contained 42.03% Fe and the $CuFeS_2$ sample contained 33.51% Cu, suggesting that the purity of FeS_2 and $CuFeS_2$ ranged from 93% to 97%. Sodium ethylxanthate (EX) and $KMnO_4$ were supplied by Shanghai Aladdin Biochemical Technology Co., Ltd. The pH of the slurry was adjusted using dilute sodium hydroxide (NaOH) and hydrochloric acid (HCl) solutions, both at a concentration of 5×10^{-5} mol/dm^3. All solutions were prepared using deionized (DI) water, and the experiments were conducted at 23°C.

Table 1 Elemental concentration of mineral samples as measured by the XRF technique

Mineral	S	Fe	Cu	Pb	Mg	Al	Si	Ca	Zn
FeS_2	48.34	42.03	-	0.11	0.98	0.59	1.34	1.3	-
$CuFeS_2$	29.43	27.08	33.51	1.33	-	0.91	2.32	-	0.09

2.2. Single mineral flotation tests

2g of pure mineral particles (0.038−0.074 mm) were conditioned with 40 mL of solution in a flotation tank of the XFG II machine. The air flow rate during the flotation process was maintained at 0.33 m^3/h, and the stirring speed was set to 1500 rpm. In the context of the traditional flotation procedure, mineral

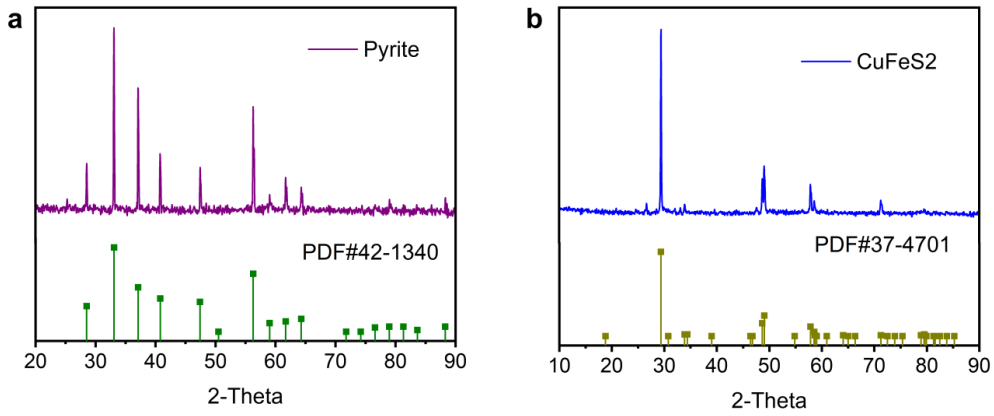

Fig. 1. XRD data for (a) FeS_2 and (b) $CuFeS_2$ samples used in this work. The standard PDF cards of FeS_2 (#42-2340) and $CuFeS_2$ (#37-4701) are plotted for comparison

particles were subjected to $KMnO_4$ for 3 min and EX for 2 min in the flotation cell. Furthermore, 7 µL of terpilenol was employed as a frother and injected into the slurry, with a conditioning time of 1 min.

In the combined treatment, 2 g of either FeS_2 or $CuFeS_2$ was reacted with $KMnO_4$ solution in the tank under ultrasound at a frequency of 120 kHz for 3 min. Subsequently, this slurry was transferred to the flotation tank (40 mL), where EX and terpilenol were also added, with treatment times for these reagents of 2 min and 1 min, respectively. The ultrasonic equipment was procured from Hangzhou Successful Ultrasound Equipment Co., Ltd., operating at a frequency of 120 kHz and a transducer power range of 0-100 W.

2.3. Contact angle determinations

A JY-82C system (China) was employed to determine the contact angles using the sessile-drop technique. Sandpapers of 80 and 1500-grit were utilized to polish the crystal surface (10×10 mm) to create a fresh surface. Subsequently, the crystal was immersed in 50 mL of $KMnO_4$ solution for a specified duration without stirring, while the solution was subjected to 120 kHz ultrasound irradiation. A DI water droplet was then gradually released by a spring to attach to the crystal surface. A camera was employed to capture images of the droplet spreading on the crystal surface for contact angle analysis, with three droplets introduced onto the crystal surface in each test.

2.4. Electrokinetic tests

FeS_2 or $CuFeS_2$ powder (0.1 g, < 5 µm) was reacted with 50 mL of solution for 5 min under stirring at 500 rpm. For ultrasonic treatment, a 120 kHz ultrasound was employed during the reaction of the mineral with the solution. Subsequently, 5 mL of the solution containing mineral powder was collected for measurement. A Nano ZSP system was utilized to determine the electrophoretic mobility of the mineral powder, with zeta potentials calculated using the instrument's software. In addition, a KCl solution at a concentration of 1×10^{-3} mol/dm^3 was employed to prepare the solution, thereby maintaining ionic strength.

2.5. XPS experiments

The XPS spectra of the mineral powder were acquired using a PHI5000 Versaprobe II. Both broad and detailed spectra were recorded and analyzed using MultiPak Spectrum software. In addition, the C 1s spectrum with a binding energy (BE) of 284.8 eV was employed to calibrate the detailed XPS spectra for subsequent fitting processes. Mineral powders (1 g, −38 µm) were reacted with the $KMnO_4$ solution (100 mL, 3×10^{-4} mol/dm^3) and subjected to ultrasonication for 1 min.

2.6. SEM-EDS analysis

The elemental distribution on the surfaces of FeS_2 and $CuFeS_2$ was examined using a JEOL JSM-6360 instrument (20 kV accelerating voltage). FeS_2/$CuFeS_2$ (2 g, 38−74 µm) was reacted with 40 mL of $KMnO_4$

solution for 1 min to prepare the sample. The mineral powder was rapidly filtered and stored in a nitrogen-filled container to prevent oxidation in air.

3. Results and discussion

3.1. Mineral flotation behavior under untrasonication

3.1.1. Effect of ultrasonic power

It is proposed that 120 kHz of ultrasonic treatment could enhance the depression of FeS_2 with $KMnO_4$. However, ultrasonic intensity serves as a key parameter determining the sonication results (Cao et al., 2024a). Therefore, the flotation responses of FeS_2 and $CuFeS_2$ to ultrasonic intensity were first evaluated in this section. Given that pH 7 is optimal for the reaction of $KMnO_4$ with FeS_2 (Cao et al., 2024b), the pH of the $KMnO_4$ solution was adjusted to 7.

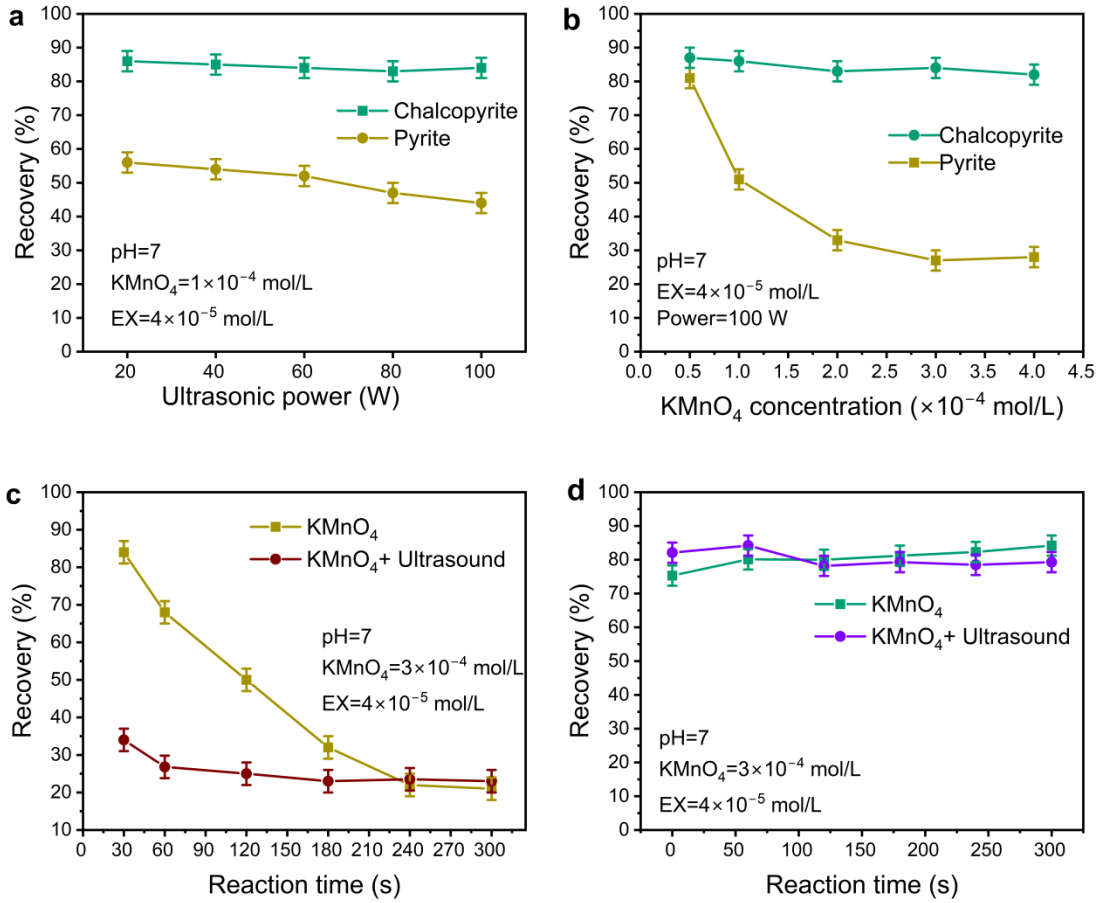

Fig. 2. Flotation responses of FeS_2 and $CuFeS_2$ as a function of: (a) ultrasonic power; (b) $KMnO_4$ concentration: reaction time (c−FeS_2, d−$CuFeS_2$)

For $CuFeS_2$, the recoveries ranged from 80% to 90% across the entire ultrasonic power range (20-100 W), as shown in Fig. 2a. This finding suggests that ultrasonic treatment had a limited effect on the flotation of $CuFeS_2$. In contrast, for FeS_2, the recovery was only 56.31% when treated with ultrasound and 1×10^{-4} mol/dm^3 of $KMnO_4$. Notably, natural FeS_2 demonstrates good floatability at pH 7 (Cao et al., 2024b). It appears that the combined treatment of $KMnO_4$ and ultrasound resulted in depression effects on FeS_2 flotation, leading to a reduction in FeS_2 recovery. Additionally, as ultrasonic power increased from 20 W to 100 W, the recovery of FeS_2 declined sharply. The recovery at 100 W (44%) was 12.32% lower than that at 20 W, indicating that ultrasonication could assist in the depression of FeS_2 with $KMnO_4$.

However, the beneficial effect of ultrasound is not substantial. This phenomenon may be attributed to two factors. Firstly, the concentration of $KMnO_4$ might be relatively low, resulting in inadequate

depression capability. Secondly, the depression effect of $KMnO_4$ is contingent upon its oxidation capacity to decrease the hydrophobicity of the FeS_2 surface. The reaction time may be insufficient for the oxidation of the FeS_2 surface. Therefore, the differences in flotation responses between FeS_2 and $CuFeS_2$ concerning ultrasonication time and $KMnO_4$ concentration on the flotation behaviors of FeS_2 and $CuFeS_2$ were further evaluated through flotation tests in the subsequent section.

3.1.2. Effect of $KMnO_4$ concentration and reaction time

Fig. 2b illustrates the flotation recoveries of FeS_2 and $CuFeS_2$ at a concentration of 4×10^{-5} mol/dm^3 of EX, contingent upon the concentration of $KMnO_4$. The ultrasonic power employed in this experiment was 100 W. The recovery of $CuFeS_2$ ranged from 80% to 90% across the entire $KMnO_4$ concentration region (5×10^{-5} to 4×10^{-4} mol/dm^3), indicating that the combined conditioning did not inhibit the flotation of $CuFeS_2$. Conversely, the elevation of $KMnO_4$ concentration resulted in a significant reduction in FeS_2 recovery, which decreased to only 27.09% at a concentration of 2×10^{-4} mol/dm^3. This finding suggests that the flotation of FeS_2 was effectively inhibited at this $KMnO_4$ concentration. Previous studies indicate that a concentration of 4×10^{-4} mol/dm^3 of $KMnO_4$, with a reaction time of 3 min, is necessary for effective depression of FeS_2 (Cao et al., 2024b). It appears that 120 kHz ultrasonication may lower the required $KMnO_4$ dosage in the separation of FeS_2 and $CuFeS_2$.

Prior research has demonstrated that ultrasonic irradiation induces a hot-spot effect within the flotation system, which may enhance the oxidation kinetics on the PbS surface, thereby reducing the conditioning time required for H_2SO_4 depressant (Cao et al., 2024a). A similar phenomenon may be applicable to the flotation of FeS_2. This section evaluates the influence of ultrasonic reaction time on the recovery of FeS_2, and the flotation behavior of FeS_2 treated solely with $KMnO_4$ was also assessed for comparative purposes.

When FeS_2 was treated with $KMnO_4$ without ultrasonication, the recovery was 86.33% at a reaction time of 30 s (Fig. 2c), indicating that the flotation of FeS_2 could not be effectively inhibited within such a short reactive period. Furthermore, the recovery of FeS_2 diminished to 23.51% as the reaction time extended to 4 min. These results demonstrate that a duration of 4 min is required for 3×10^{-4} mol/dm^3 of $KMnO_4$ to effectively depress FeS_2. In contrast, the recovery of FeS_2 significantly decreased when ultrasound was applied during $KMnO_4$ treatment. After 30 s of combined treatment, the recovery fell to 34.36%, representing a 52% reduction compared to treatment with $KMnO_4$ alone. Moreover, with 60 s of ultrasonic irradiation, the recovery further decreased to 27.81%, a value comparable to that observed after 4 min of $KMnO_4$ treatment. These findings elucidate that ultrasound substantially reduces the reaction time necessary to inhibit FeS_2 flotation. The propagation of ultrasound generates hot spots on the FeS_2 surface, with temperatures reaching 4000-5000 K, which significantly enhances the oxidative rate of the FeS_2 surface.

In addition, the effect of ultrasonic duration on the flotation response of $CuFeS_2$ was examined, as summarized in Fig. 2d. Specifically, the $KMnO_4$ treatment, with or without ultrasonication, did not alter the $CuFeS_2$ recovery as the reaction time increased from 0 to 5 min. These flotation results further illustrate that ultrasound does not enhance the depression of $CuFeS_2$ by $KMnO_4$. Therefore, ultrasound may aid in the separation of FeS_2 from $CuFeS_2$.

The flotation results indicate that ultrasonic treatment improved the oxidation efficiency of FeS_2 with $KMnO_4$. Therefore, ultrasonication reduced the reaction time to 1 min, which is 75% shorter than the reaction time (4 min) without ultrasound.

3.2. Hydrophobicity analysis

Neutral FeS_2 can be readily floated by EX due to its high surface hydrophobicity (Cao et al., 2023a). The hydrophobicity of FeS_2 may be diminished by $KMnO_4$ treatment, attributed to the oxidation effect of $KMnO_4$. The contact angles of FeS_2 and $CuFeS_2$ treated with ultrasound and $KMnO_4$ were measured to evaluate the effect of ultrasonication on the hydrophobicity of the minerals. The experimental parameters included 3×10^{-4} mol/dm^3 of $KMnO_4$ and 100 W ultrasonication.

It was observed that water droplets did not spread on the $CuFeS_2$ surface, resulting in a contact angle of 75.3° (Fig. 3), consistent with previous reports (Cao et al., 2024a). Moreover, $KMnO_4$ treatment marginally reduced the contact angle of $CuFeS_2$, which remained approximately 70° after 5 min of

$KMnO_4$ treatment. Furthermore, the contact angle of the $CuFeS_2$ surface was still 62.4° after 5 min of combined treatment with ultrasound and $KMnO_4$. Ultrasonication did not significantly diminish the hydrophobicity of $CuFeS_2$. These results suggest that ultrasonication had a minimal effect on the hydrophobicity of $CuFeS_2$, corroborating the earlier flotation results.

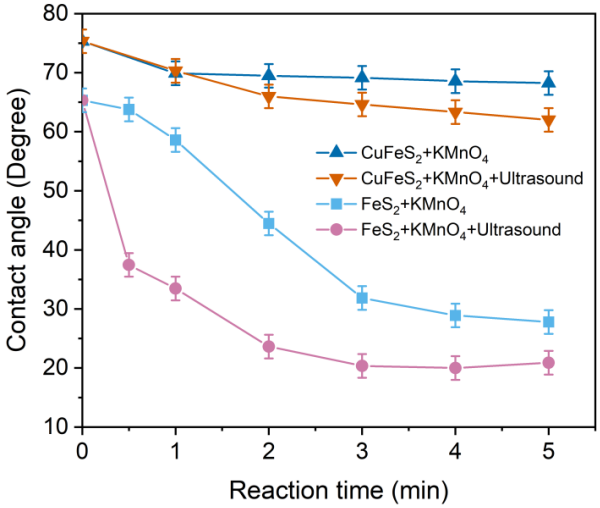

Fig. 3. Contact angles of FeS_2 and $CuFeS_2$ surfaces as a function of reaction time of $KMnO_4$ and ultrasonication (The $KMnO_4$ concentration was 3×10^{-4} mol/dm^3 for the measurement.)

In terms of FeS_2, the contact angle measured was 65.3°, which represents a reduction of 7° compared to the value observed for the original $CuFeS_2$ surface. Furthermore, the contact angle for FeS_2 was significantly decreased following $KMnO_4$ treatment, reaching 27.8° after 5 min of reaction. Additionally, a contact angle of 33.5° was achieved after 1 min of combined $KMnO_4$ and ultrasound treatment, with individual $KMnO_4$ treatment requiring 3 min to yield similar results. Moreover, a 2-min combined treatment decreased the contact angle to 23.6°, which is 4° lower than that achieved with 5 min of $KMnO_4$ treatment. The interaction of $KMnO_4$ with the FeS_2 surface generates hydrophilic oxygen (O)-bearing species (Cao et al., 2024b).

Ultrasonication appears to facilitate the interaction between $KMnO_4$ and FeS_2, resulting in the formation of oxidative species in a shorter duration (1 min). The beneficial effects of ultrasound may arise from its hot spot effect, which induces localized high-temperature regions on the FeS_2 surface. It is predicted that these elevated temperature areas could significantly accelerate the oxidative reactions on the FeS_2 surface, leading to a reduction in the required oxidation time.

3.3. Zeta potential study

The zeta potential investigation was conducted to examine the adsorption of the EX^- anion on the FeS_2 and $CuFeS_2$ surfaces treated with $KMnO_4$ and subjected to 120 kHz ultrasound. The $KMnO_4$ concentration utilized for conditioning was 3×10^{-4} mol/dm^3.

For the FeS_2 sample in DI water, an increase in pH resulted in the presence of OH^- anions on its surface, which lowered the zeta potential (Fig. 4a). The point of zero charge was determined to be within the pH range of 5 to 6. At pH 7, the zeta potential exhibited a more negative value (−22.71 mV) when FeS_2 was reacted with EX, in contrast to the value in DI water at the same pH. This observation indicates that EX^- anions interacted with the FeS_2 surface at pH 7. Furthermore, the zeta potential increased to −0.20 mV at pH 7, when FeS_2 was treated with 3×10^{-4} mol/dm^3 of $KMnO_4$ and subjected to ultrasonication. This suggests that the oxidative components on the FeS_2 surface enhance its zeta potential. A similar trend was reported in previous studies (Khoso et al., 2019). However, for the FeS_2 treated with $KMnO_4$ and ultrasonication, the presence of EX did not alter the zeta potential of FeS_2 at pH 7. This finding suggests that the EX^- anion could not adsorb onto the oxidative FeS_2 surface, which may account for the limited recovery of FeS_2.

For $CuFeS_2$, the zeta potential measured at pH 7 was −16.13 mV. Moreover, the zeta potential of $CuFeS_2$ with EX at pH 7 was observed to be −10 mV lower than that in DI water. This finding indicates

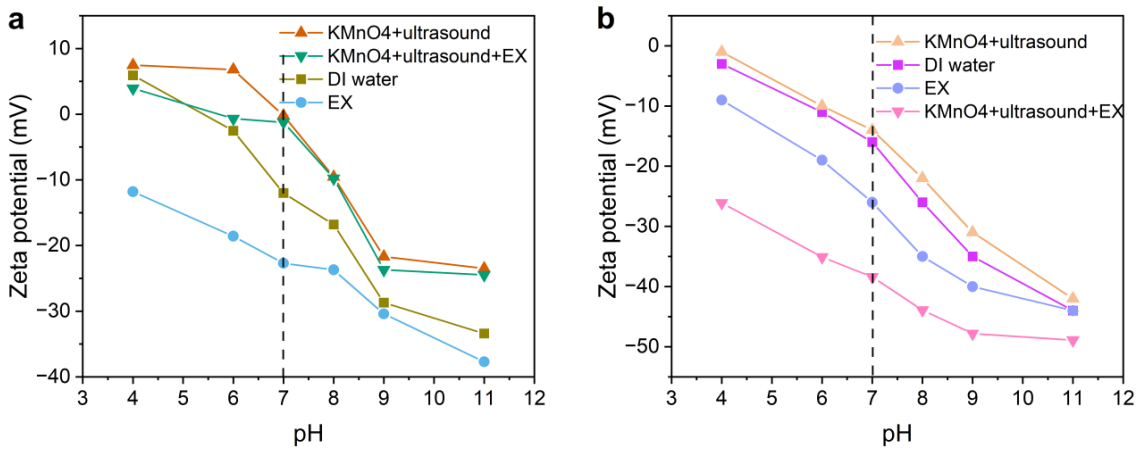

Fig. 4. Zeta potential results of FeS_2 (a) and $CuFeS_2$ (b) samples ($KMnO_4$ and EX concentrations in the tests were 3×10^{-4} mol/dm^3, and 4×10^{-5} mol/dm^3.).

that the EX^- anion can adsorb onto the $CuFeS_2$ surface. The combined treatment at pH 7 resulted in an increase of only 2 mV in zeta potential compared to that of $CuFeS_2$ in water at pH 7. The application of $KMnO_4$ and ultrasound treatment did not alter the surface composition of the $CuFeS_2$. When $CuFeS_2$ was treated with $KMnO_4$, ultrasonication, and EX, its zeta potential at pH 7 was found to be 24 mV lower than that of the sample treated solely with $KMnO_4$ and ultrasonication. These results indicate that the combined treatment with $KMnO_4$ and ultrasound did not inhibit the adsorption of EX^- onto the $CuFeS_2$ surface. Notably, the zeta potential of $CuFeS_2$ reacted with EX was also 12 mV lower than that of natural $CuFeS_2$ in EX solution. Ultrasonic conditioning seems to facilitate the interaction of EX^- anions with the $CuFeS_2$ surface by potentially removing surface coatings, thereby promoting reactions with the $CuFeS_2$.

Our zeta potential data elucidate that the combined treatment of $KMnO_4$ and ultrasound did not impede the adsorption of the EX^- anion onto the $CuFeS_2$ surface. Conversely, this treatment generated oxidative species on the FeS_2 surface, which inhibited the reaction of the EX^- anion with the FeS_2 surface.

3.4. Surface components determination

$KMnO_4$ treatment induces oxidation reactions on the FeS_2 surface, leading to the formation of oxidative components (Cao et al., 2024b). Typically, ultrasound irradiation can eliminate gangue and oxidative minerals from mineral surfaces through strong microjets (Xu et al., 2017). However, the aforementioned zeta potential experiments demonstrate that, within the FeS_2-$KMnO_4$ system, ultrasound actually facilitated the formation of surface oxides. To further verify whether ultrasound exhibited surface cleaning behavior, the XPS technique was utilized to analyze changes in the chemical environments of atoms on mineral surfaces resulting from the reactions induced by ultrasonication and $KMnO_4$.

The binding energy (BE) of the Fe $2p_{3/2}$ level in bulk FeS_2 was determined to be 707.41 eV, which aligns well with previous findings (Khoso et al., 2019). The combined treatment resulted in the emergence of an additional Fe component on the FeS_2 surface, exhibiting a BE of 711.34 eV. This component was identified as FeO/FeOOH according to prior reports (Chimonyo et al., 2017; Xian et al., 2015). However, the proportion of this component constituted only 17.43% of all Fe species, indicating that the oxidation of Fe is not the primary factor contributing to the depression of FeS_2. Regarding the S spectra, the S $2p_{3/2}$ peak at 162.63 eV corresponded to S in the bulk FeS_2, while the peak at a higher S $2p_{3/2}$ BE of 169.04 eV was attributed to SO_4^{2-} species (Sun et al., 2023). The concentration of SO_4^{2-}, however, was only 9.32% of all Fe atoms. These XPS results demonstrate that a slight oxidation occurred on the original FeS_2 surface. As FeS_2 underwent the combined treatment, the peak at 168.97 eV became more pronounced, with the concentration of SO_4^{2-} increasing to 26.54%. This elevated percentage of SO_4^{2-} suggests that oxidative components remained on the FeS_2 surface following ultrasound irradiation, which contributes to the reduction in the hydrophobicity of FeS_2.

Additionally, the detailed spectra of $CuFeS_2$ samples were analyzed and summarized in Fig. 6. For natural $CuFeS_2$, the BEs of Cu $2p_{3/2}$ and Fe $2p_{3/2}$ were 932.51 eV and 708.21 eV, respectively. Furthermore,

an additional Fe peak at 721.71 eV in the natural $CuFeS_2$ surface was attributed to the Fe-O species resulting from surface oxidation (Sun et al., 2024). However, the application of ultrasonic waves and $KMnO_4$ did not significantly increase the percentage of Fe-O species, with an increase of only 3%. In terms of S species, two surface species were identified on the original $CuFeS_2$ surface, namely S^{2-} (S $2p_{3/2}$ BE = 161.51 eV) and S_n^{2-} (S $2p_{3/2}$ BE = 163.75 eV) (Bai et al., 2022; Huang et al., 2019). These two components were also observed in the spectrum after treatment with ultrasound and $KMnO_4$, and no other species were detected. These XPS findings confirm that the combined treatment did not generate new oxidative species on the $CuFeS_2$ surface.

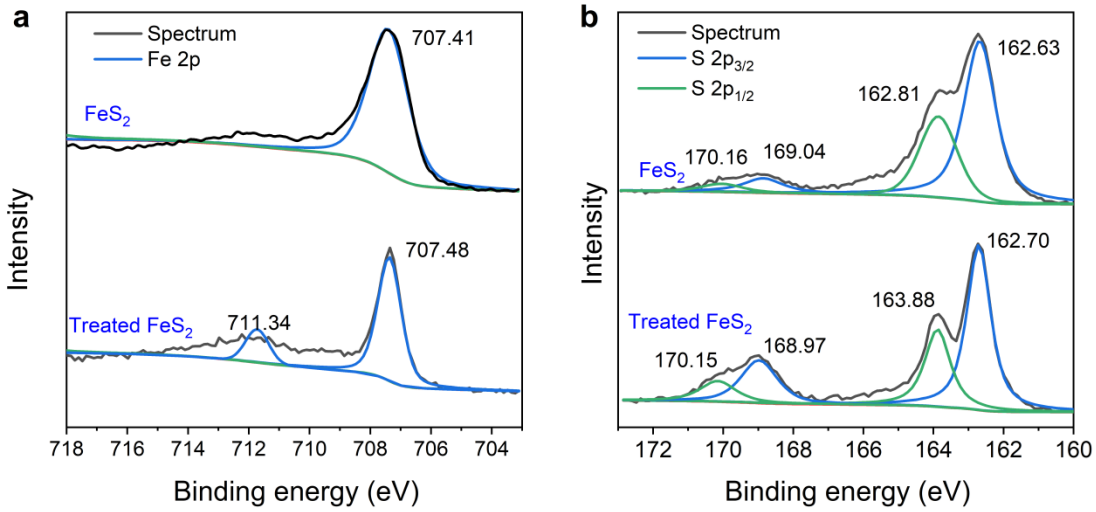

Fig. 5. XPS results of natural FeS_2 and FeS_2 treated by $KMnO_4$ and ultrasonication (The ultrasonic power and $KMnO_4$concentration were 100 W and 3×10^{-4} mol/dm^3 during the reaction.)

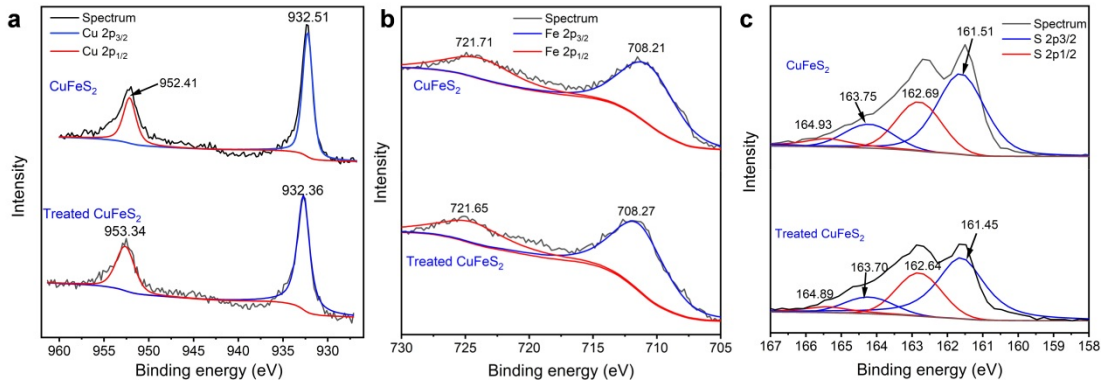

Fig. 6. XPS results of elements on the natural and treated $CuFeS_2$ samples, including Cu (a), Fe(b), and S(c). (The ultrasonic power and $KMnO_4$ concentration were 100 W and 3×10^{-4} mol/dm^3 during the reaction.)

3.5. SEM-EDS study

The SEM-EDS system is widely utilized to analyze the microscopic morphology of solid surfaces, with magnification capabilities reaching up to 500,000 times (Feng et al., 2019). This technique also allows for the determination of surface atomic concentrations of elements, with a detection limit of 0.1% for elements with atomic numbers higher than carbon (Chen et al., 2023). In mineral oxidation studies, SEM-EDS has been successfully employed to investigate elemental changes on mineral surfaces, such as in the PbS-H_2SO_4 system. Given the advantages of SEM-EDS, elemental distribution on mineral surfaces was assessed using this methodology.

Fig. 7a summarizes the elemental concentrations on the original FeS_2 surface. Notably, the O percentage was measured at 4.47% (Table 2). This relatively low concentration of O atoms may result from oxidative species present on the natural FeS_2 surface, as the FeS_2 surface is susceptible to oxidation by atmospheric O and moisture (Wen et al., 2025). Furthermore, the O atomic percentage increased to

14.15% following the combined treatment. The presence of FeO, FeOOH, and SO_4^{2-} components accounts for the elevated O concentration, as corroborated by the aforementioned XPS results. In addition, the distribution of O species was observed throughout the entire examined area (Fig. 7b), indicating that the FeS_2 surface may be extensively covered by oxidative components.

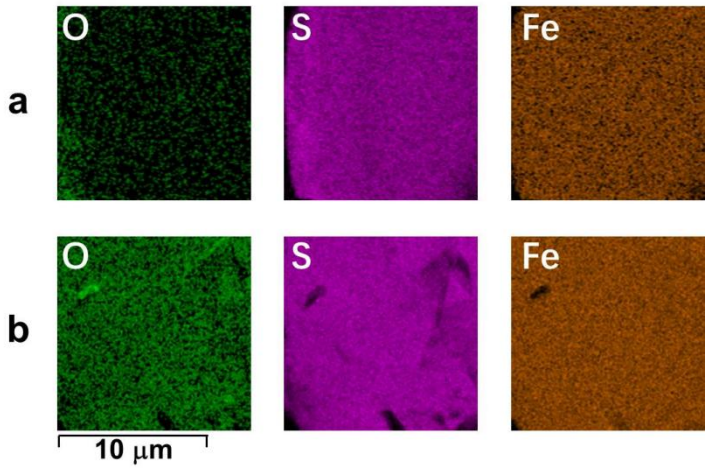

Fig. 7. Elemental concentrations on the natural (a) and treated (b) FeS_2 surface measured by the SEM-EDS technique

The elemental concentrations on the $CuFeS_2$ surfaces are compared in Fig. 8. For each analyzed element, namely Cu, Fe, S, and O, the $KMnO_4$ and ultrasound treatment did not result in significant variations in their concentrations. Specifically, the change in concentration was less than 3%. In contrast, the concentration of O increased by 3.42% following the reaction with $KMnO_4$ and ultrasonication. This limited increase in O concentration is unlikely to markedly enhance the hydrophilic properties of the $CuFeS_2$ surface.

In summary, our XPS and SEM-EDS results indicate that 1 min of $KMnO_4$ treatment combined with ultrasonication enhances the oxidation degree of the FeS_2 surface. This combined conditioning leads to the production of iron oxides on the FeS_2 surface, which subsequently diminishes its hydrophobicity. However, the oxidation degree of the $CuFeS_2$ surface remained unchanged. Thus, ultrasonic treatment may be effectively applied in the separation process of FeS_2 from $CuFeS_2$.

In addition, it should be stressed that the application of $KMnO_4$ causes some environmental concerns. Moreover, $KMnO_4$ is more expensive than conventional pyrite depressants, such as lime. Therefore, we will explore cheaper and more environmentally-friendly depressants in the future and investigate whether ultrasound can produce a synergistic effect with these depressants.

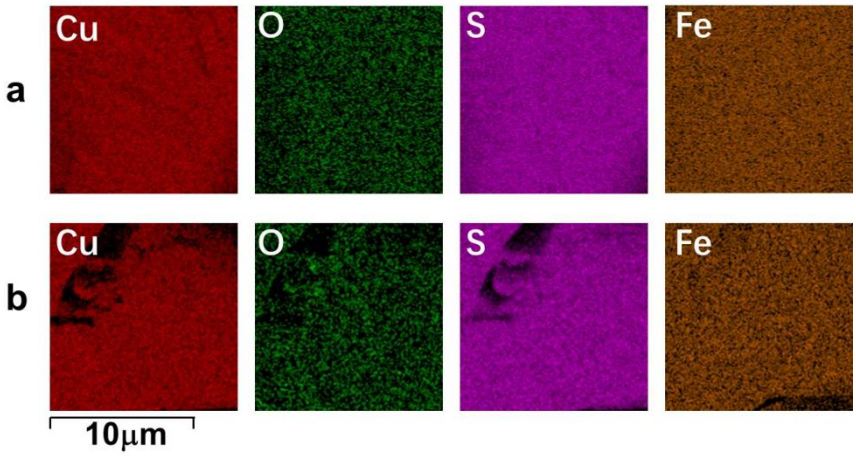

Fig. 8. Elemental concentrations on the natural (a) and treated (b) $CuFeS_2$ surface measured by the SEM-EDS technique

Table. 2 Element concentrations (%) measured by the EDS technique

	O	Fe	S	Cu
Natural FeS_2	4.47	43.37	52.16	
Treated FeS_2	14.15	30.97	54.85	
Natural $CuFeS_2$	9.28	20.96	41.37	28.36
Treated $CuFeS_2$	5.86	23.47	41.30	29.36

4. Conclusions

Ultrasonic treatment at 120 kHz has the potential to enhance the separation of FeS_2 from $CuFeS_2$ by froth flotation when utilizing $KMnO_4$ as an oxidant. The combination of ultrasonication and $KMnO_4$ significantly reduces the reaction time required for the depression of FeS_2. Therefore, the recovery of FeS_2 was only 27.81% after 1 min of treatment with a concentration of 3×10^{-4} mol/dm^3 and an ultrasonic power of 100 W.

This combined treatment resulted in the presence of FeO, FeOOH, and SO_4^{2-} components on the FeS_2 surface, leading to a marked decrease in FeS_2 hydrophobicity. Furthermore, the O percentage on the FeS_2 surface increased by 9.68% due to the coating of oxidative components. The beneficial effect of ultrasonication is primarily attributed to the cavitation phenomenon, which generates hot spots in the slurry, thereby accelerating the rate of the oxidative reaction. In contrast, this combined treatment did not result in the adherence of oxidative species to the $CuFeS_2$ surface. Therefore, ultrasonication at 120 kHz can be effectively employed for the separation of these two minerals.

Acknowledgments

The present work is supported by the National Engineering and Technology Research Center for Development & Utilization of Phosphate Resources (NECP-2024-13) and the Intelligent Mining and Green Separation Technology (202305AK340002).

References

ALTUN, N., HWANG, J., HICYILMAZ, C., 2009. *Enhancement of flotation performance of oil shale cleaning by ultrasonic treatment.* Int. J. Miner. Process. 91, 1-13.

ASHOKKUMAR, M., 2011. *The characterization of acoustic cavitation bubbles–An overview*. Ultrason. Sonochem. 18, 864-872.

ASHOKKUMAR, M., CRUM L., FRENSLEY C., GRIESER F., MATULA T., MCNAMARA W., SUSLICK K., 2000. *Effect of Solutes on Single-Bubble Sonoluminescence in Water*. J. Phys. Chem. A. 104, 8462-8465.

ASHOKKUMAR, M., GRIESER F., 2005. *A comparison between multibubble sonoluminescence intensity and the temperature within cavitation bubbles.* J. Am. Chem. Soc. 127, 5326-5327.

BAI, X., LIU J., FENG Q., WEN S., DONG W., LIN Y., 2021. *Study on selective adsorption of organic depressant on chalcopyrite and pyrite surface*s. Colloids Surf., A. 627, 127210.

BAI, X., LIU J., WEN S., LIN Y., 2022. *Selective separation of chalcopyrite and pyrite using a novel organic depressant at low alkalinity.* Miner. Eng. 185, 107677.

BARMA, S.D., BASKEY, P.K., RAO, D.S., SAHU, S.N., 2019. *Ultrasonic-assisted flotation for enhancing the recovery of flaky graphite from low-grade graphite ore.* Ultrason. Sonochem. 56, 386-396.

CAO, Q., LI Y., ZOU H., LIU D., Y., ZHANG H., 2024. *Synergistic effects of ultrasonication on the flotation separation of galena from chalcopyrite using sulfuric acid as a depressant*. Miner. Eng. 206, 108501.

CAO, Q., YAN W., LIU D., WEN S., LI Y., 2023. *New insights into pyrite-hydrogen peroxide interactions during froth flotation: experimental and DFT study*. Physicochem. Probl. Miner. Process. 59, 157409.

CAO, Q., ZHANG H., YAN Y., LI Y., LIU D., 2023. *Flotation separation of pyrite and chalcopyrite with potassium permanganate as a depressant.* Chem. Pap. 78, 1761-1773.

CELIK, M.S., 1989. *Effect of Ultrasonic Treatment on the Floatability of Coal and Galena.* Sep. Sci. Technol. 24, 1159-1166.

CHEN, J., LI Y., CHEN Y., 2011. *Cu–S flotation separation via the combination of sodium humate and lime in a low pH medium.* Miner. Eng. 24, 58-63.

CHEN, Y., CHEN Y., LIU Q., LIU X., 2023. *Quantifying common major and minor elements in minerals/rocks by economical desktop scanning electron microscopy/silicon drift detector energy-dispersive spectrometer (SEM/SDD-EDS).* Solid Earth Sci. Libr. 8, 49-67.

CHEN, Y., TRUONG, V., BU, X., XIE, G., 2020. *A review of effects and applications of ultrasound in mineral flotation*. Ultrason. Sonochem. 60, 104739.

CHIMONYO, W., WIESE J., CORIN K., O'CONNOR C., 2017. *The use of oxidising agents for control of electrochemical potential in flotation.* Miner. Eng. 109, 135-143.

FENG, B., ZHANG W., GUO Y., WANG T., LUO G., WANG H., HE G., 2019. *The flotation separation of galena and pyrite using serpentine as depressant.* Powder Technol, 342, 486-490.

FILIPPOV, L.O., FILIPPOVA, I.V., BARRES, O., LYUBIMOVA, T.P., FATTALOV, O.O., 2021. *Intensification of the flotation separation of potash ore using ultrasound treatment*. Miner. Eng. 171, 107092.

GUNGOREN, C., BAKARHAN, Y., DEMIR, I., OZKAN, S.G., 2020. *Enhancement of galena-potassium ethyl xanthate flotation system by low power ultrasound.* Trans. Nonferrous Met. Soc. China. 30, 1102-1110.

GUNGOREN, C., OZDEMIR, O., WANG, X., OZKAN, S.G., MILLER, J.D., 2019. *Effect of ultrasound on bubble-particle interaction in quartz-amine flotation system.* Ultrason. Sonochem. 52, 446-454.

HAN, G., WEN S., WANG H., FENG Q., 2019. *Effect of starch on surface properties of pyrite and chalcopyrite and its response to flotation separation at low alkalinity*. Miner. Eng. 143, 106015.

HASSANZADEH, A., HASANZADEH M., 2017. *Chalcopyrite and pyrite floatabilities in the presence of sodium sulfide and sodium metabisulfite in a high pyritic copper complex ore*. J. Dispersion Sci. Technol. 38, 782-788.

HUANG, X., HUANG K., JIA Y., WANG S., CAO Z., ZHONG H., 2019. *Investigating the selectivity of a xanthate derivative for the flotation separation of chalcopyrite from pyrite.* Chem. Eng. Sci. 205, 220-229.

KHOSO, S., HU Y., LÜ F., GAO Y., LIU R., SUN W., 2019. *Xanthate interaction and flotation separation of H2O2-treated chalcopyrite and pyrite*. Trans. Nonferrous Met. Soc. China. 29, 2604-2614.

LIU, D., ZHANG G., CHEN Y., HUANG G., GAO Y., 2020. *Investigations on the utilization of konjac glucomannan in the flotation separation of chalcopyrite from pyrite.* Miner. Eng. 145, 106098.

MARQUES, M.L.S., FILIPPOV, L.O., FILIPPOVE, I.V., SILVA, L.A., PRATES, L.M., PEREIRA, A.M., CORREIA, J.C.G., 2025. *Concentration of goethitic slimes by comprehensively exploring a ternary Collector-Frother flotation reagent and ultrasound dispersion*. Sep. Purif. Technol. 354, 128633.

MITRA, S., HOQUE M., EVANS G., NGUYEN A., 2021. *Direct visualisation of bubble-particle interactions in presence of cavitation bubbles in an ultrasonic flotation cell*. Miner. Eng. 174, 107258.

MU, Y., PENG Y., LAUTEN R., 2018. *The galvanic interaction between chalcopyrite and pyrite in the presence of I lignosulfonate-based biopolymers and its effects on flotation performance.* Miner. Eng., 122, 91-98.

NIE, G., HU K., REN W., ZHOU P., WANG S., 2021. *Mechanical Agitation Accelerated Ultrasonication for Wastewater Treatment: Sustainable Production of Hydroxyl Radicals*. Water Res. 198, 117124.

OWUSU, C., FORNASIERO D., ADDAI-MENSAH J., ZANIN M., 2014. *Effect of regrinding and pulp aeration on the flotation of chalcopyrite in chalcopyrite/pyrite mixtures.* Powder Technol. 267, 61-67.

SUN, ., YU J., ZHANG W., LI P., LI Y., HAN Y., 2024. *Flotation separation of chalcopyrite from pyrite and sphalerite using a novel collector: An experimental and mechanism investigation*. Appl. Surf. Sci. 661, 160059.

SUN, Y., LYU H., GAI L., SUN P., SHEN B., TANG J., 2023. *Biochar-anchored low-cost natural iron-based composites for durable hexavalent chromium removal.* Chem. Eng. J. 476, 146604.

WEN, Z., SHI X., SUI H., ZHANG M., ZHANG L., GU Y., FENG Q., MA K., ZHANG N., WANG M., ZHANG R., XU C., LI Z., XUE R., 2025. *Air oxidation behavior of wet-mechanochemically synthesized pyrite FeS2: Fenton performance regulated by Fe species, sulfur vacancy and crystal facet ratio.* Chem. Eng. J. 509, 161166.

WU, S., WANG J., TAO L., FAN R., WANG C., SUN W., GAO Z., 2022. *Selective separation of chalcopyrite from pyrite using an acetylacetone-based lime-free process.* Miner. Eng. 182, 107584.

XIAN, Y., WANG Y., WEN S., NIE Q., DENG J., 2015. *Floatability and oxidation of pyrite with different spatial symmetry.* Miner. Eng. 72, 94-100.

XU, M., XING, Y., GUI, X., CAO, Y., WANG, D., WANG, L.,2017. *Effect of Ultrasonic Pretreatment on Oxidized Coal Flotation.* Energy Fuels, 31, 14367-14373.

YAN, H., YUAN Q., ZHOU L., QIU T., AI G., 2018. *Flotation kinetics and thermodynamic behavior of chalcopyrite and pyrite in high alkaline systems.* Physicochem. Probl. Miner. Process. 54, 901-910.

ZANIN, M., LAMBERT H., DU P., 2019. *Lime use and functionality in sulphide mineral flotation: A review*. Miner. Eng., 143, 105922.

ZHANG, H., ZHANG F., SUN W., CHEN D., CHEN J., WANG R., HAN M., ZHANG C., 2023. *The effects of hydroxyl on selective separation of chalcopyrite from pyrite: A mechanism study*. Appl. Surf. Sci. 608, 154963.